ENTE PER LE NUOVE TECNOLOGIE,
L'ENERGIA E L'AMBIENTE

Associazione EURATOM-ENEA sulla Fusione

INERTIAL CONFINEMENT PHYSICS AND TECHNOLOGY GROUP PROGRESS REPORT (1994-1995)

RT/ERG/FUS/96/18

This report has been prepared and distributed by: Servizio Edizioni Scientifiche - ENEA
Centro Ricerche Frascati, C.P. 65 - 00044 Frascati, Rome, Italy

SUMMARY

The technical activities performed during the period 1994-1995 in the framework of the Inertial Fusion Physics and Technology Group, are reported. The theoretical and numerical work, as well as experiments performed with the Frascati ABC facility are described.

(INERTIAL CONFINEMENT FUSION, LASER COMPRESSED D-T FUEL, IGNITION BY EXTERNAL INJECTED TRIGGER, NUMERICAL LAGRANGIAN CODE, LASER MATTER INTERACTION, X-RAY PLASMA DIAGNOSTICS, OPTICAL PLASMA DIAGNOSTICS)

RIASSUNTO

Sono riportate le attività tecnico-scientifiche svolte dall' Unità Fisica e Tecnologia della Fusione Inerziale nel biennio 1994-1995. Viene descritto il lavoro teorico e numerico assieme a quello sperimentale svolto con l'impianto ABC di Frascati.

INDEX

INERTIAL CONFINEMENT PHYSICS AND TECHNOLOGY GROUP PROGRESS REPORT (1994-1995)

OUTLINE AND OVERVIEW *(A. Caruso)*

This report outlines the technical activities performed, during the last two years (1994-1995), in the framework of the Inertial Fusion Physics and Technology Group. The entrusted task is to maintain a critical evaluation capability on energy-oriented inertial confinement fusion (ICF) in the context of the ENEA-EURATOM Association. Theoretical and numerical work as well as experiments with the ABC facility were performed. A watching-brief minor activity on rising topics related to laser ICF drivers, was devoted to new solid-state laser amplifier pumping methods.

The experimental activity was mainly oriented to critically reviewing relevant ICF issues as, e.g., studies on the possibility of getting smooth, spatially uniform acceleration over distances many 10 times the in-flight-foil-thickness (IFFT). These studies have shown several interesting features.

In the experiments performed with the ABC facility, the laser light was focused on the target by plain F/1 aspherical lenses. It has been experimentally found, and then theoretically justified, that the imprinting of non-homogeneity in the target illumination does not produce foil distortions as the target evolves. Actually a sort of stabilization occurs due to *refractive interchange* during the initial 1-D corona formation. These processes are quite fast and may occur within the transit time of the first shock wave through the foil. The theoretical studies clearly demonstrate the decay of the first shock deformation to wavelengths 1/2 of the initial perturbation wavelength, with subsequent no substantial deviation of the fluid motion from a quasi 1-D flow.

The induced spatial incoherence (ISI) technique has been applied to produce very good smooth and uniform on-target energy deposition. Actually on-target energy density depositions have been generated in which the amplitude of the space modes with $n \geq 6$ results below 1%, whereas that of modes with $n \geq 10$ is set to about 0.1%. These results have been obtained in the near field by adding to the main focusing optics, arrays of square negative lenses with

random thickness (256 lenses per array). Taking for IFFT the theoretical value, and for the displacement the measured one, smooth foil acceleration over distances of the order of 100×IFFT have been obtained. To set an upper limit to the value of the IFFT, exploratory work based on foils collision was carried out.

In very preliminary tests, we have made two SiO_2 foils (4 μm thick) to collide after a flight of 100-150 μm each. This has been obtained by irradiating, from opposite directions, two parallel foils mounted 200-300 μm apart. If two foils are made to collide after a 100 μm flight the theoretical analysis shows that, in a time of the order of 100 ps the foil temperature, T_{rad}, is rised from a few thousands degrees to about 5×10^5 °K. The thickness of each foil is reduced by a factor about 4. As the power of the radiation emitted scales as T_{rad}^4 a bright flash of radiation will be emitted, for a time of the order of 100 ps, from a region ≈1μm thick.

In the framework of the experimental activity described in the following, some original method for time-resolved soft x-ray 2-D imaging was carried out. Also, referring to the description of electronic heat transport, some hints on normalizing the Lagrangian 1-D and 2-D codes (CoMo3 and CoBi3) were obtained as a by-product of the experiments.

Inertial confinement fusion, is a scheme in which no external fuel confinement is involved. In this approach, energy release (by fusion of light nuclei) is obtained by the propagation through *unconfined, highly compressed fuels* of a *burn wave* generated by *an ignition spark.* Fuel burn is limited by *system disassembling* (due to unbalanced pressure). In those civilian contexts in which only energy-oriented research is pursued, the approach is often labelled as "inertial fusion energy" (IFE).

In ICF the high fuel densities needed are obtained in spherical implosions, which are produced by applying *pressure pulses* to the external surface of a solid, millimeter-sized spherical fuel container. Common to most of the ICF schemes is the idea of generating the required high pressures by the high temperature blow-off (ablation) of the container outer layers.

In the approach extensively adopted by the most important ICF programs ignition is provided by *a single* spark *self-generated by the implosion process itself,* near the implosion symmetry center.

In the past and recently recovered, another possibility has been considered, the one based on the *injection* of the ignition spark *in the compressed fuel* by an additional (short) energy pulse.

In this approach a mass of DT fuel is compressed along a cold adiabat by a properly tailored laser pulse, and ignited at stagnation by an externally injected trigger. The trigger could be provided by a short burst of soft x rays, or by an extremely low emittance heavy-ion beam [1], by a macroparticle impact [1], or by a burst of high-energy electrons produced by an ultra-short laser pulse [2], etc.

Historically, the injected ignition spark scheme was the first to be considered in the open literature. The coupling of ablative compression to an injected ignition spark was the scheme

most studied at Frascati within the EURATOM-ENEA Association in the period 1966-1970 (on this see, e.g., a review on the macroparticle impact approach in [3], a study of the hydrodynamics induced by laser ablation in [4], scaling laws for the parameters of the hot spark created in dense matter by ultra-short laser pulses in [5], and the description of an experiment performed by irradiating solid deuterium by ultra-short laser pulses in [6]).

Although at the initial development stages, the injected spark approach can take advantage of all the theoretical and experimental methods set up since the first proposals, in the sixties. In the different variants, this scheme is potentially relevant for the development of IFE, since it promises such high gains, to relax the efficiency requirements for drivers to acceptable values.

In this context the quality (symmetry) of the implosion may be not substantially relevant, since the interest lies in the achievement of high average densities. Also final fuel mixing is not a relevant process because the ignition spark is injected.

During the last two years, the new ICF schemes based on injected spark were considered relevant topics to be explored by theoretical activity and numerical simulations.

1. REPORT ON THE ABC ACTIVITY

1.1. Interaction-experiment features (A. Caruso, C. Strangio)

The ABC facility includes a two-beam neodymium glass laser (driven by a 0.15 THz bandwidth glass oscillator) [7], an appropriate focusing optics (a smoothing system being available), diagnostics and a small area for target preparation. The Neodymium glass laser powering the facility is characterized by:

- maximum power density: 3×10^{15} W/cm^2 (by F/1 optics);
- minimum spot size: 40 μm;
- FWHM duration (fig. 1a): 3 ns;
- operating wavelength: 1.054 μm
- optional 2 ω conversion

The two laser beams are focused on the target throughout two (holed) aspherical F/1 lenses (focal length=10 cm) placed inside the vacuum chamber. A suitably designed array [8,9] composed of random thickness lenses (beam integrator) may be easily coupled to (or removed from) each F/1 lens for near field ISI smoothing (fig. 1b). As shown in the figure, the interaction experiments were performed with circularly polarized light.

The time-integrated energy distributions in the focal region at full laser power, for the two possible illumination modes, *without* and *with* arrays, are reported in figures 2a and 2b.

The diagnostics in the ABC installation are aligned according to the scheme shown in figure 3a. The interaction area is probed by four light pulses (300 ps, λ=0.527 μm, t_1, t_2 , t_3, t_4 in fig. 3a), independently synchronizable between -1 ns and +15 ns with respect to the beginning of the interaction pulses ramp. Each channel can be individually processed to produce dark-field shadowgraphs, interferograms and streak images (with 2 ps resolution) of the shadows, or in self-emitted visible light. The optical resolution of these channels is about 10 μm.

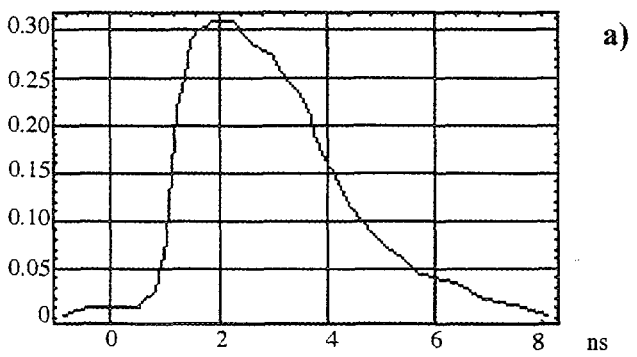

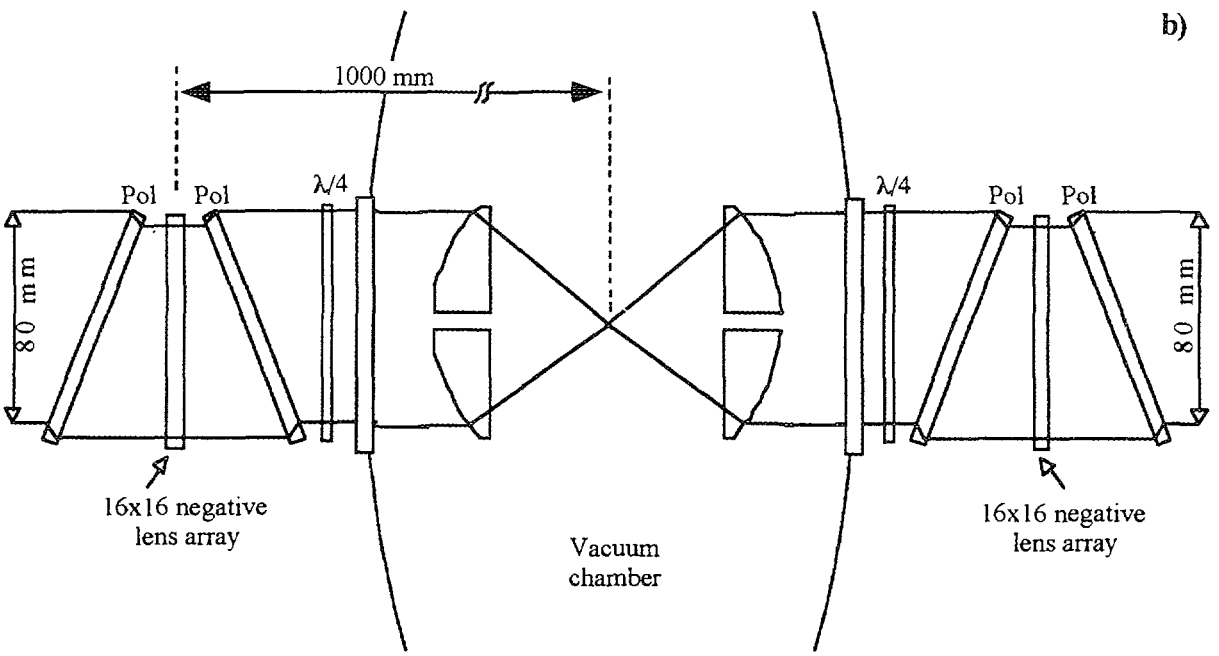

Fig. 1 - Power time dependence of the ABC laser pulses (a). The final optics in the ABC installation. Two arrays of negative square lenses with random thickness can be inserted to produce near-field ISI smoothing at the focus of the two F/1 aspherical lenses (b).

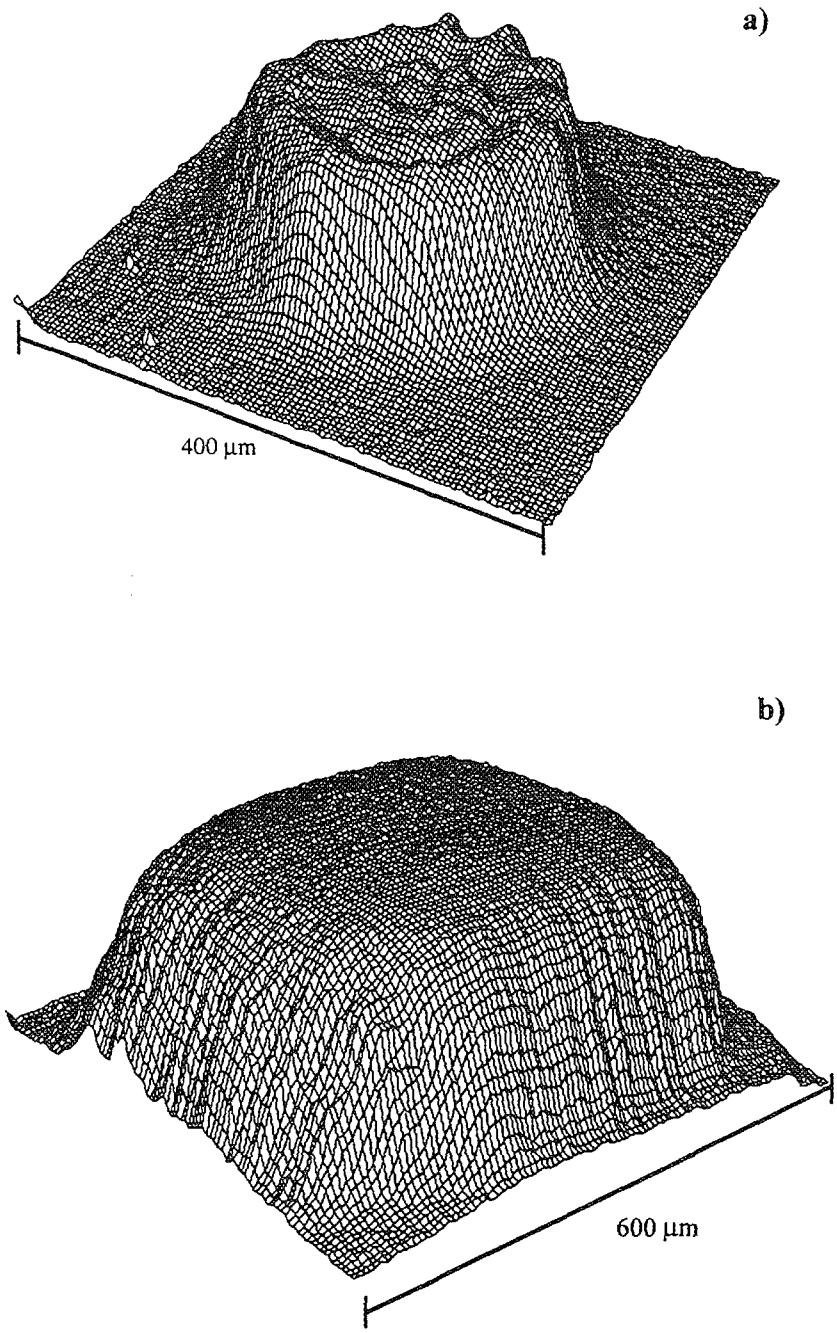

Fig. 2 - The measured energy density profile, at full laser power, without arrays (a) and with arrays (b). The measurements were made on spot magnified images produced by one of the F/1 focusing lenses. Calibrated N/P Polaroid plates were used as recording media, by exploiting their two-photon absorption.

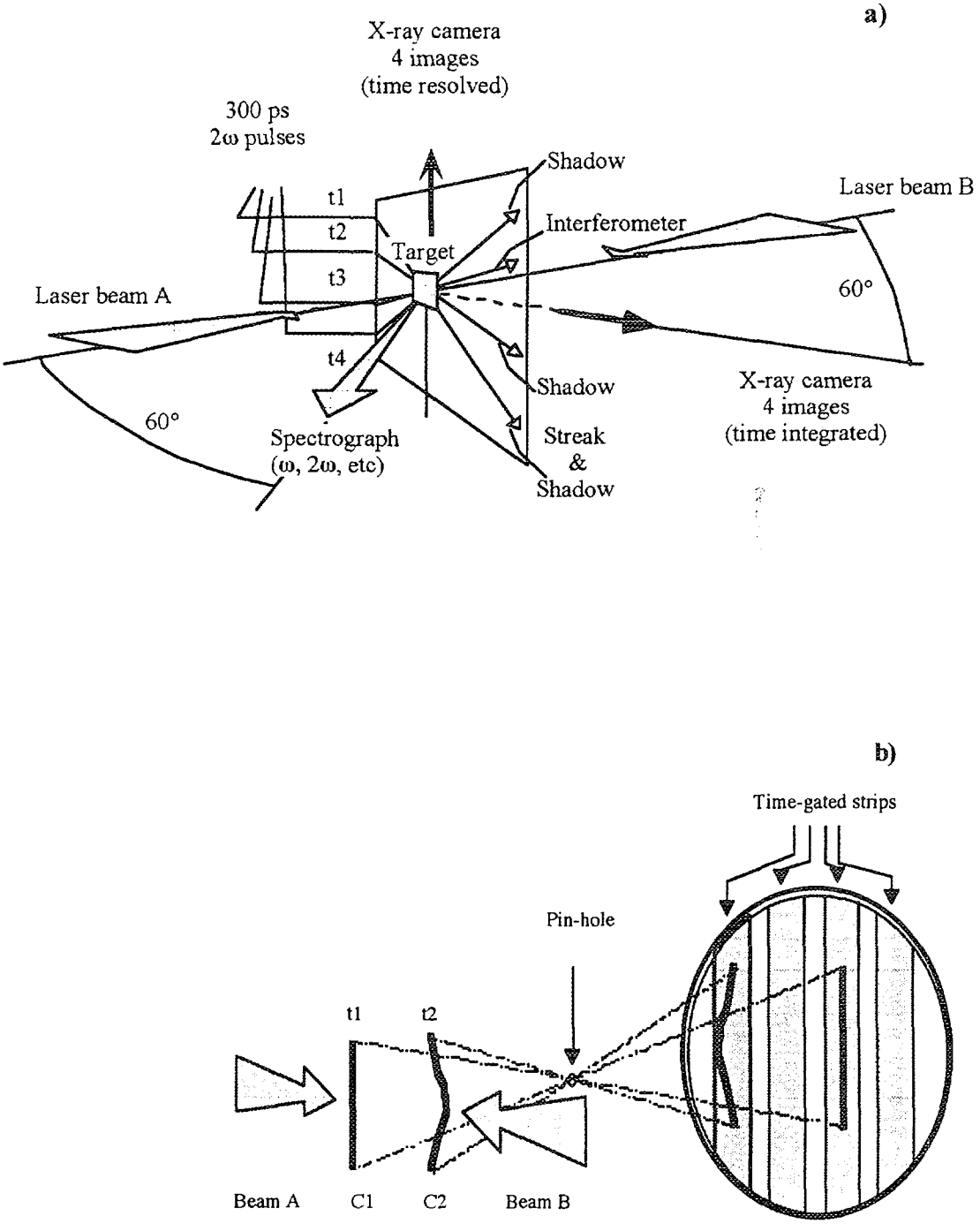

Fig. 3 - General layout of diagnostics and irradiation geometry used in the experiments. Imaging is arranged to produce time-resolved side views of the target (a). Time resolved x-ray imaging for the dense phase evolution. A target passing from configuration C1 at time t1 to configuration C2 at time t2, is imaged trough a single pinhole on the time gated strip lines (b).

Four time-integrated and differently filtered x-ray images are also taken in each shot at 120° from beam A through a 20 μm pinhole (fig. 3a).

In the same shot, at different instants with reference to the laser target interaction, four x-ray frames are also taken by a 2-D time-gated imaging system (for the dense phase evolution studies). A target passing from configuration C1 at time t1 to configuration C2 at time t2 (fig. 3b), is imaged through a single pinhole on the time gated strip lines. To take x-ray images of the dense phase motion, with delays greater than the corona x-ray emission time, the laser beam B (fig. 3b) can be operated to produce (with a selected delay respect to the driving beam A) a secondary x-ray source on the rear side of the displaced dense phase. This method results especially advantageous because it provides an initial fiducial position for the accelerated target.

Experiments, *without* and *with* ISI smoothing may be performed.

The experiments described in the following were performed by irradiating on-stalk mounted thin SiO_2 square foils (700×700×4μm) of very high optical surface quality [10] (fig. 4).

Without the lens arrays inserted, the foil surface is placed before the site of minimum focal area to produce time-integrated energy density distributions like that shown in fig. 2a. The distribution is characterized by a flat-top with modulations of about 6% in amplitude. The fairly good quality of the energy distribution is due to the low power density, and to the low amplifiers filling factor at which the ABC laser was operated.

With the arrays inserted, an across-laser-beam averaging is introduced, as well as ISI time smoothing. The schematics of this operation mode, as shown in fig. 5, were calculated with a Monte Carlo program including finite beam divergence [11]. Interference is not included on the code, since ISI time averaging is expected.

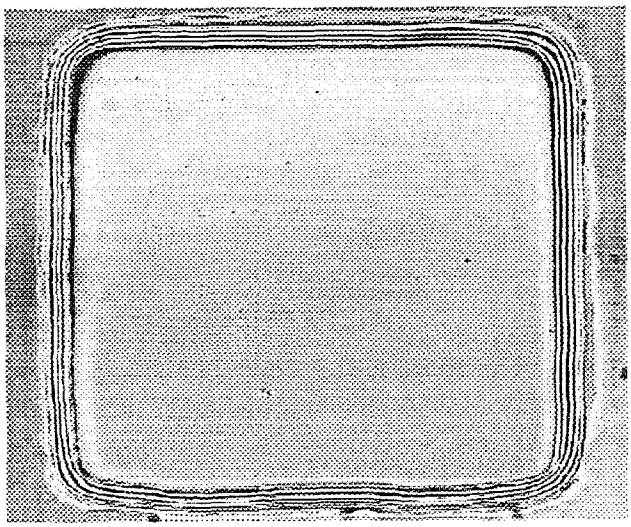

Fig. 4 - Interferometric view of a thin SiO_2 foil (700×700×4 μm) used in the experiments.

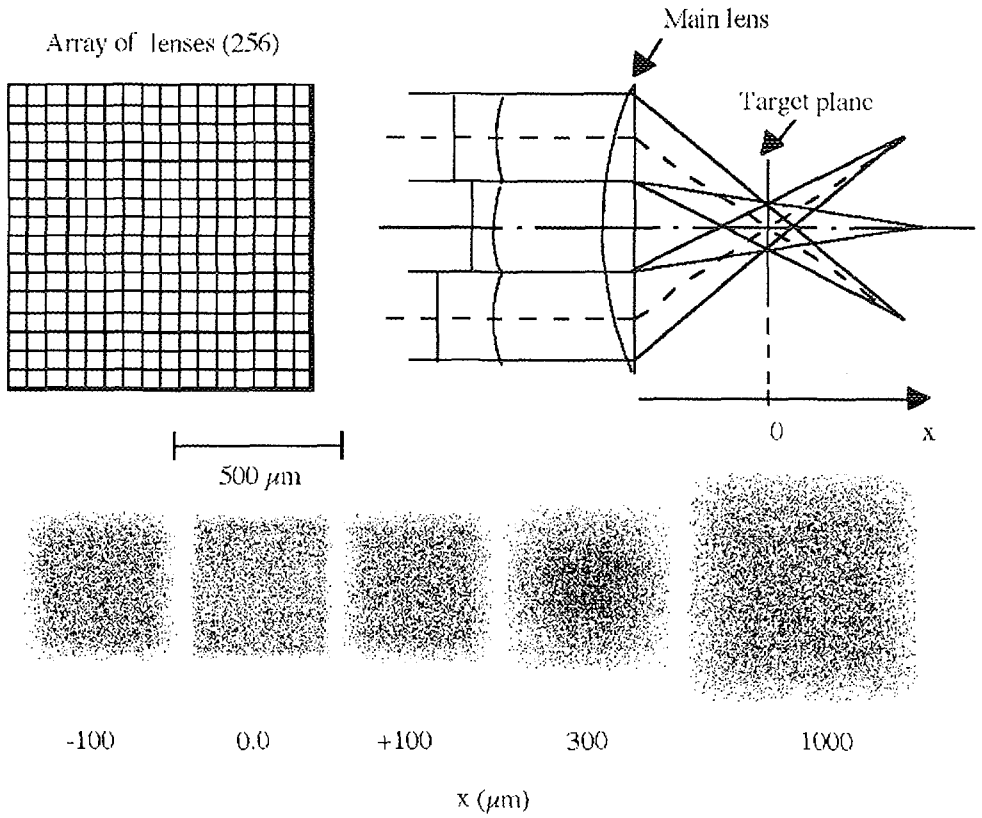

Fig. 5 - Schematics for the near-field ISI smoothing technique adopted in the ABC facility. The focal energy distributions along the main lens optical axis were obtained by a Monte Carlo simulation. Fairly flat energy distributions are obtained for a depth as much as 200 μm.

1.2. Hydrodynamic behaviour of thin foils irradiated by near-field ISI smoothed beams and foils collision experiments (P.L. Andreoli, A. Caruso, G. Cristofari, A. Dattola, P. Maci, C. Strangio)

At power densities between 5×10^{12} and 2×10^{13} W/cm^2, two illumination modes were used, one based on near-field multilens array ISI smoothing, the other on focusing by F/1 aspherical lenses (see previous section). The aim was to produce information on the evolution of thin foils accelerated over distances much greater than their in-flight thickness (say a ratio of 50÷100) in a classical, low power density regime.

The studies [12] discussed in the following are essentially based on time-resolved optical diagnostics and time-resolved x-ray imaging, both aligned for side views according to the general layout displayed in figure 3a.

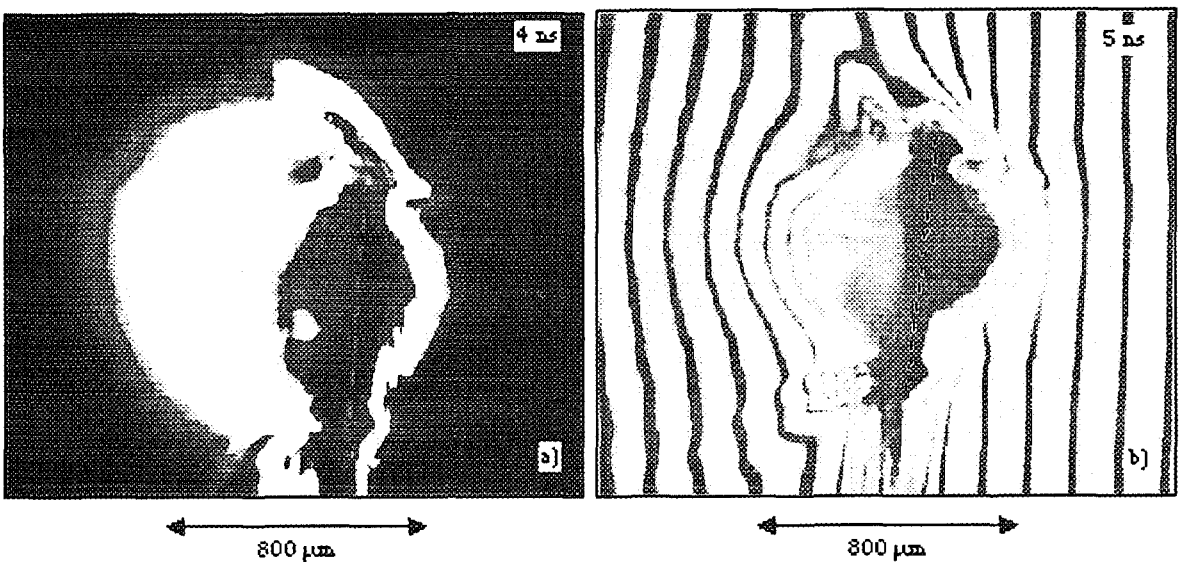

Fig. 6 - Dense phase displacement and the corona structure as observed by optical shadowgraphy (a) and optical interferometry (b) for a target accelerated with the laser pulse and focusing conditions represented in fig. 1a and 2a. The time delay is taken from the beginning of the high-power ramp of fig. 1. The straight line represents the initial target position.

Figures 6a and 6b show the optical shadowgraphy and interferometry, at different times, of a thin SiO_2 foil irradiated through the focusing lenses *without arrays*. In this situation, in spite of the 6% modulation on the illumination profile flat-top (fig. 2a), smooth dense-phase displacement was observed. This feature was maintained for a quite long time (up to ≈15 ns).

In this focusing mode the power density distribution on the target is strongly influenced by refractive effects in the corona.

Among such effects, due to the light refraction out of the higher densities, produced where the light intensity was initially higher, of special relevance is the stabilizing site interchange (*refractive interchange*) between the high- and low-intensity illumination regions.

In the experiments this mechanism was found to be very active, since no detectable trace was detected in the dense foil evolution of the 6% illumination non uniformities. For the *refractive interchange* stabilizing mechanism a simple theoretical model was made [11].

Figure 7 shows how the mechanism works inside the dense matter (by a CoBi3 simulation, see sec. 1.3). Also shown is the pressure field within a foil driven by a nonuniform beam with the power time-dependence of figure 1a.

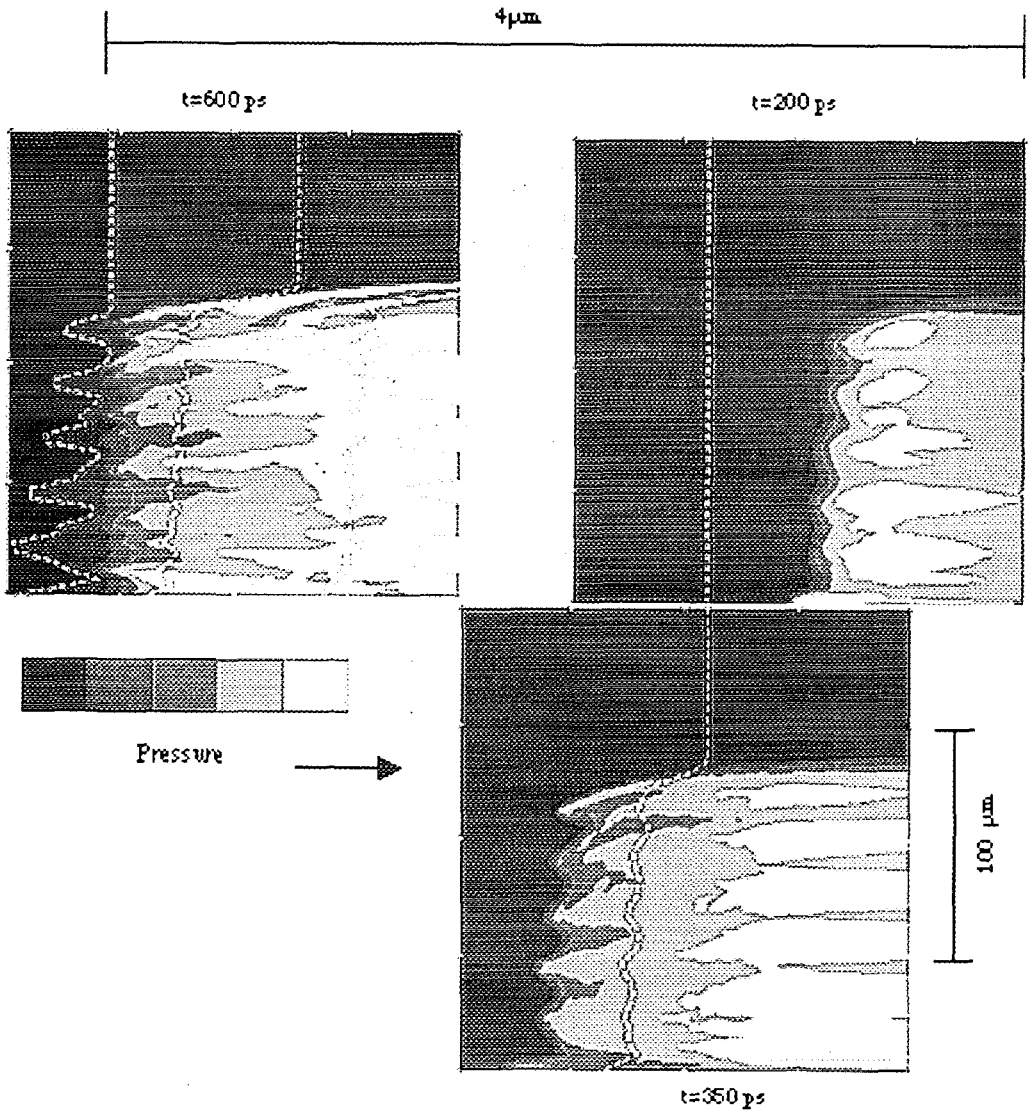

Fig. 7 - Calculated evolution of the pressure field within a foil driven by a nonuniform beam with the power time-dependence of fig. 1a. To be noted the scale difference along the two axes.

The simulation was made for a 4-μm-thick SiO_2 foil irradiated with the ABC focusing optics, *without arrays* (figs. 1b and 2a) and in cylindrical symmetry, with about five radial wavelengths on a radius of the laser profile flat-top. On the right one can note how the pressure maxima, aligned with the shock wave valleys at t=200 ps, are shifted to the peaks at 350 ps, which leads to the stabilization and wave decay shown at 600 ps.

In the explored regimes the corona x-ray emission remains intense enough to be useful for the 2-D time-resolved imaging assembly for about 1.5 ns. To take x-ray images of the dense phase motion, with delays greater than this time, the laser beam B (fig. 3b) was operated with a 4 ns (or more) delay respect to the driving beam A.

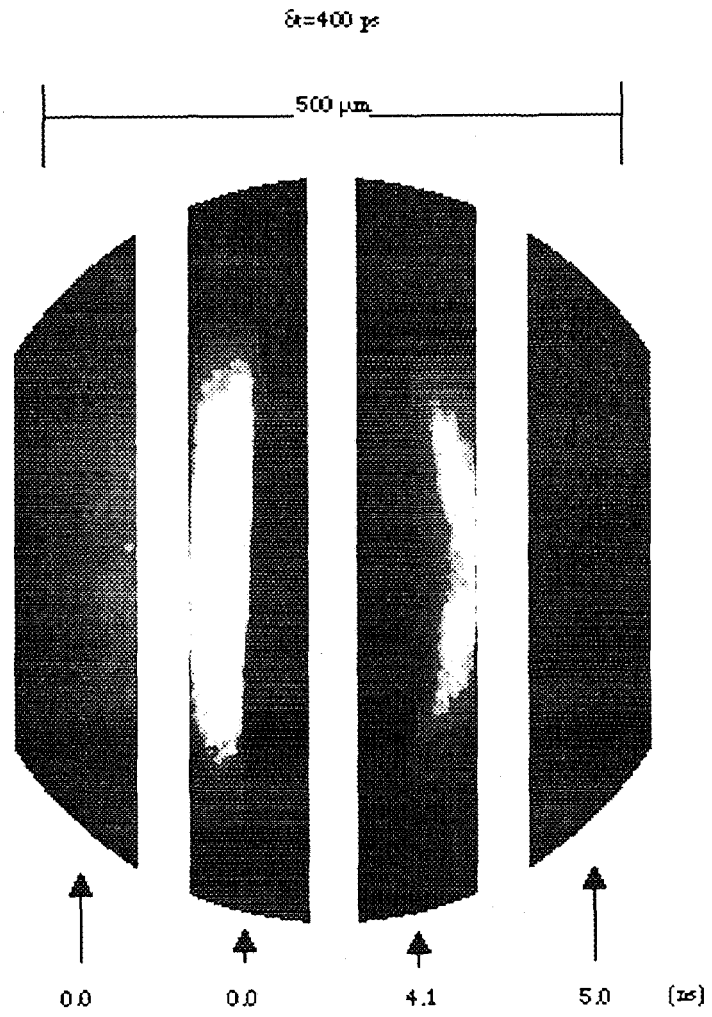

Fig. 8 - Soft x-ray imaging for a target irradiated with the nonsmoothed beams. The imaging technique is that represented in fig. 3b. As for optical diagnostics, again no effects of the nonuniformity imprinting are visible. The foil shape is revealed by the dark boundary on the third strip gated ($\delta t \approx 400$ ps) with 4.1 ns delay with respect to the start of foil irradiation.

The shape of a foil (fig. 8), taken after a displacement of about 170 μm, does not show significant effects due to the focal spot nonuniformities.

The experimental results were in very good agreement with the optical diagnostics observations.

With the lens arrays inserted, dense-phase displacements become quite planar. The resulting corona structure is also very smooth and reproducible, as clearly shown by optical diagnostics. This quite remarkable reproducibility (shot-to-shot) is demonstrated by the dark-field shadowgraphs and by the interferograms showing fields of plasma gradients very similar in both the shots (figs. 9a and 9b).

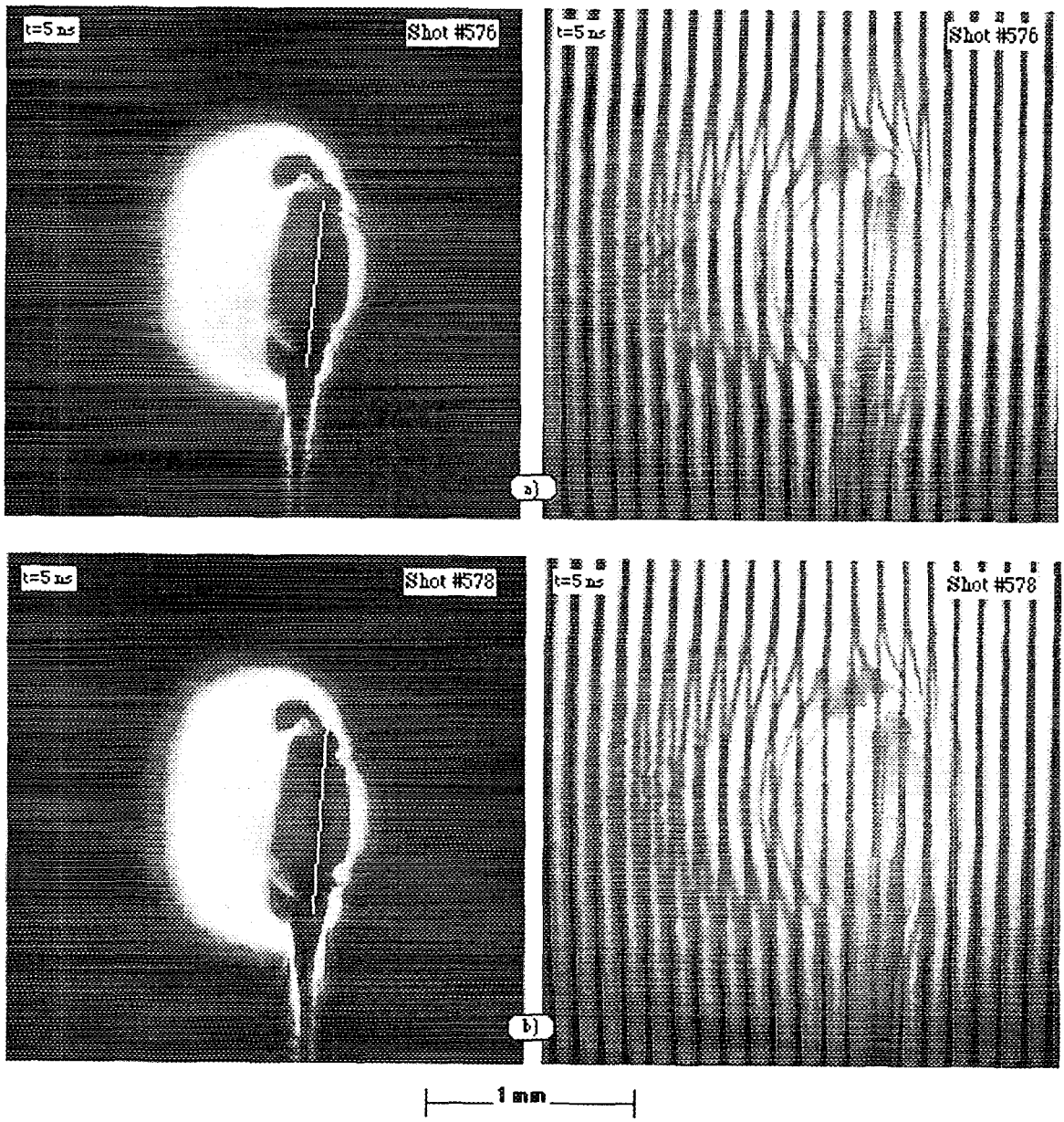

Fig. 9 - Dark-field shadowgraphs and interferograms for two consecutive on-target laser shots. The targets were irradiated with the smoothed energy distribution. In shot #576 (a) the pulse energy and foil thickness were both about 4% greater than in shot #578 (b). The dense material distribution shows a flat-top, with the same extension as that displayed by the smoothed focal energy distribution. The two shots document the very good shot-to-shot reproducibility of the foil and corona structures.

This scenario was confirmed by x-ray images, showing thin foils accelerated over 100-200 μm, and still maintaining a flat and smooth structure (fig. 10).

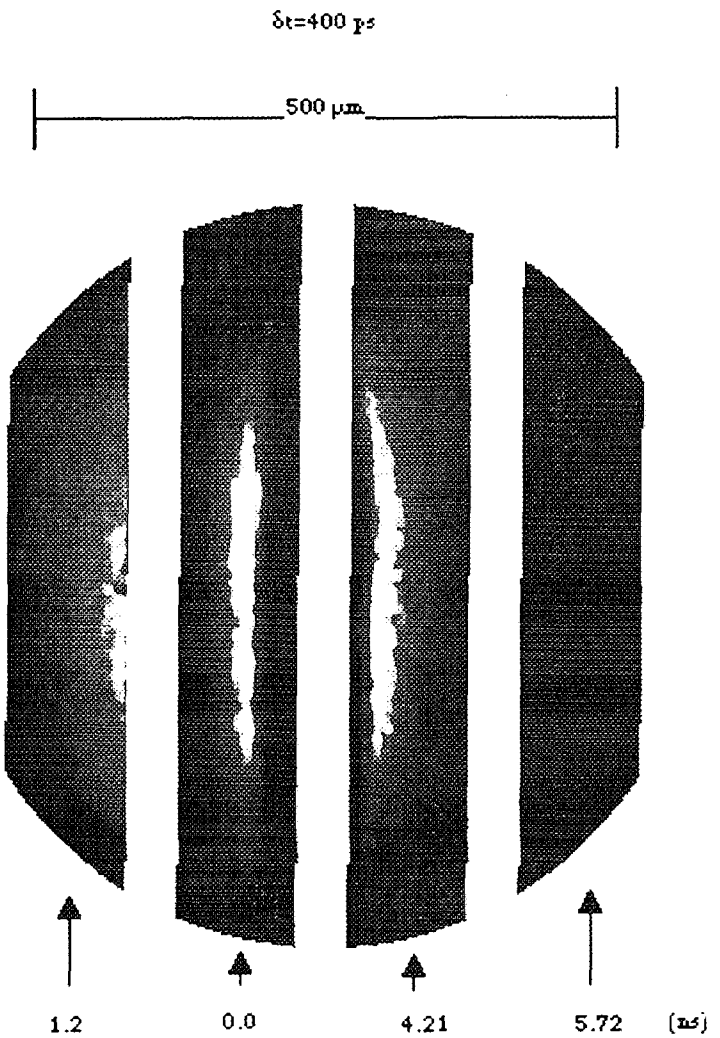

Fig. 10 - Time resolved x-ray imaging (gate time $\delta t \approx 400$ ps) for a target accelerated by a smoothed beam. After about 4 ns the foil was displaced by about 100 μm without any substantial, apparent distortion.

To set an upper limit to the value of the IFFT, exploratory work based on foils collision was carried out.

In very preliminary tests, a collision was induced between two (4 μm-thick) SiO_2 foils after a flight of 100-150 μm each. Two parallel foils mounted 200-300 μm apart were irradiated, from opposite directions, by using as drivers beams A and B operated in the smoothed mode. The diagnostics geometry is represented in figure 11; the overall collision pattern as seen by transverse dark field shadowgraphy in figure 12. A common feature of these pictures is the presence of low-density jets moving transversely to the direction of the collision. The jets could be related to a squeezing out of that low-density matter already observed in figure 9a and 9b, forerunning the dense material.

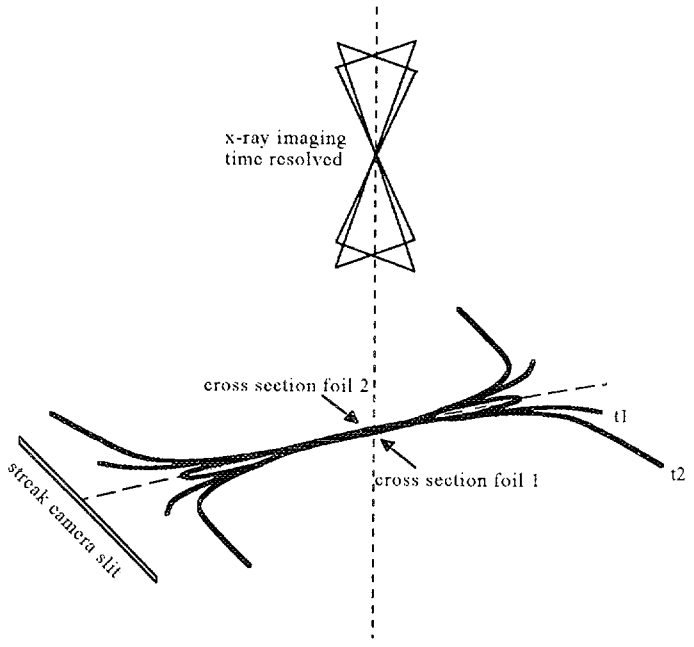

Fig. 11 - Geometry and diagnostics layout for the collision experiments.

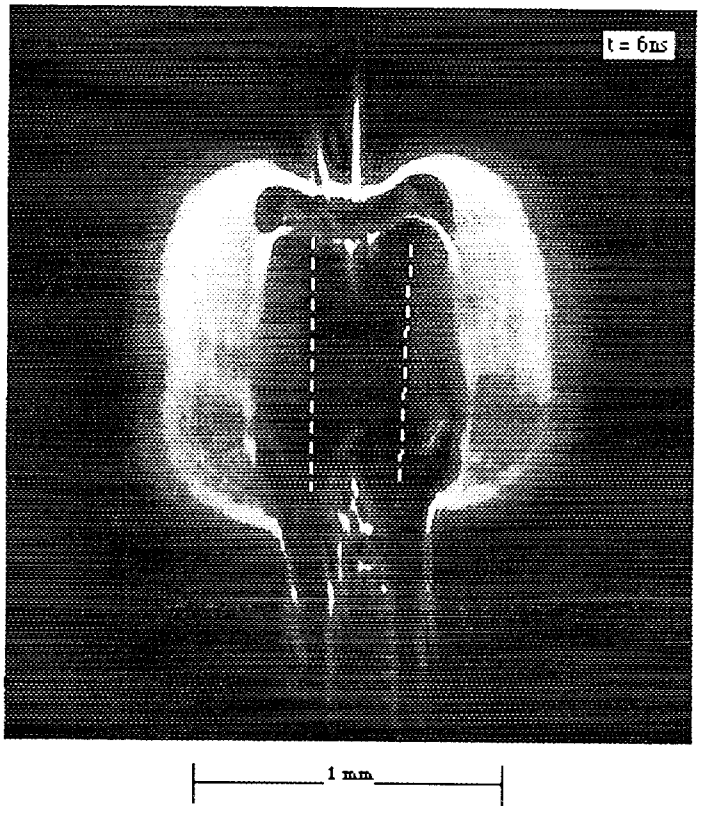

Fig. 12 - Dark field shadowgraphy of two colliding SiO_2 foils. The foils, initially ≈300 μm apart, were accelerated by two smoothed beams.

The collision process as recorded on the optical streak camera is shown in figure 13. A bright structure, with the proper duration, appears between the two foils. The pattern, as represented in terms of density levels, appears limited in size to the optical system resolution power (10-15 the theoretical IFFT) .

Similar results, as predicted by a simple shock-wave analysis, were also obtained in x-ray images (fig. 3b) taken in very preliminary tests performed at modest time resolution (1.2 ns gating time, fig. 14).

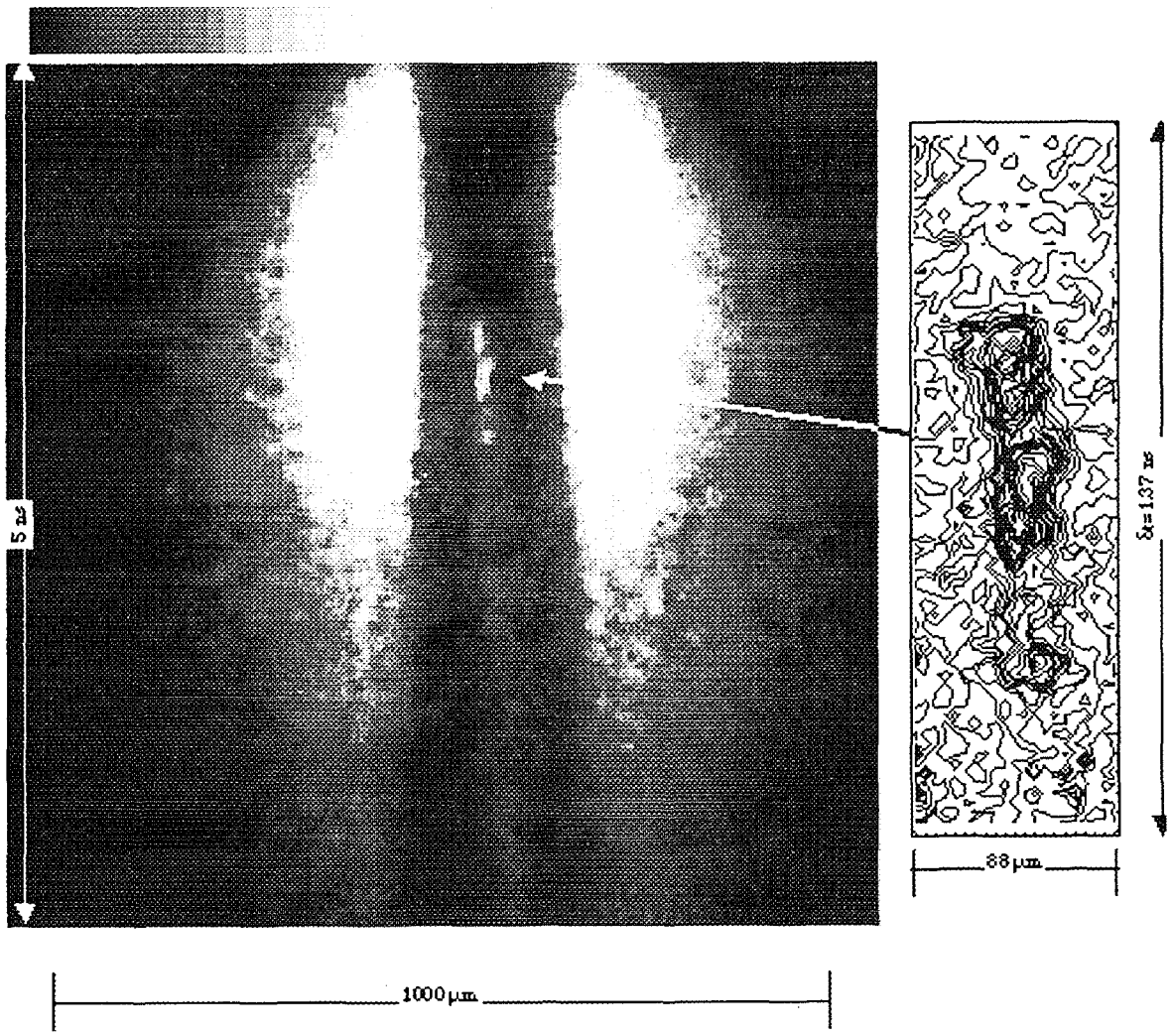

Fig. 13 - Digital streak camera record for a foil collision. The magnified view isolevels point out the production of a bright structure lasting for a few 100 ps and of the order of the diagnostic space resolution.

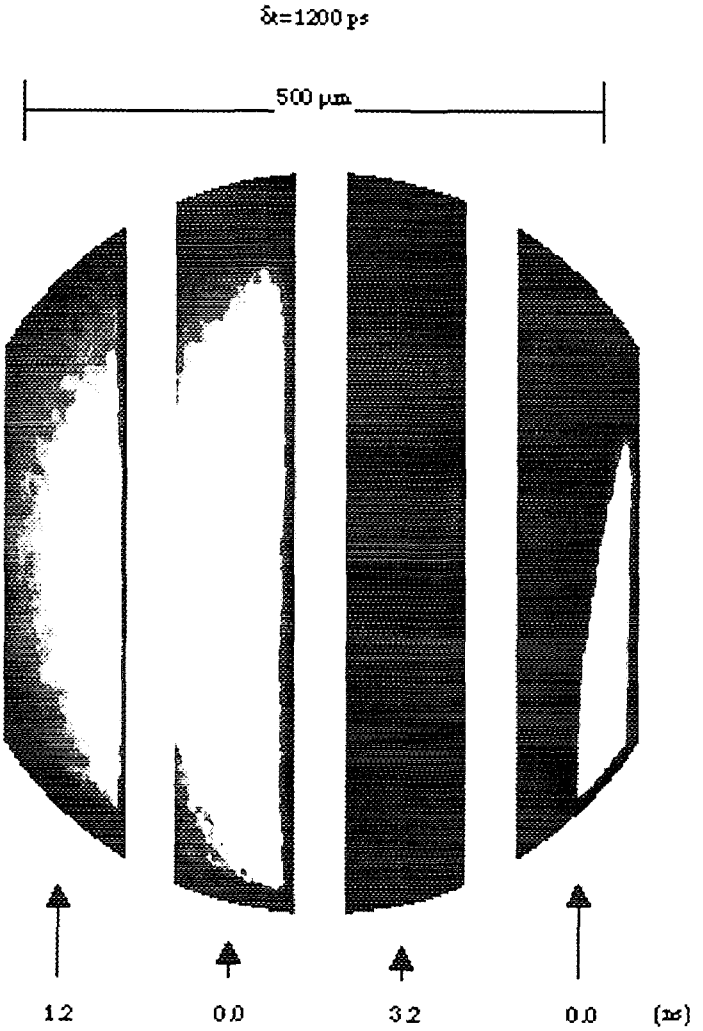

Fig. 14 - Soft x-ray imaging (gate time $\delta t \approx 1200$ ps) of a foil collision.

1.3. The CoMo3 and CoBi3 hydrodynamic codes and the physical models normalization based by experiments performed on thin SiO_2 foils irradiated with the ABC facility (A. Caruso, A.Dattola, V.A. Pais, C. Strangio)

CoMo3 and CoBi3 represent the latest version of the Lagrangian hydrocodes (1-D, CoMo and 2-D, CoBi) developed in the framework of the Inertial Fusion Physics and Technology Group activities.

In the first version (CoMo1, 1977) [13] , the evolution of matter was described by solving (implicit-iterative finite-difference method) the fluid conservation equations for two species (two temperatures), ions and electrons.

The physical models included were: flux limited thermal conduction, ion viscosity, Von Neumann artificial viscosity, local deposition of the fusion reaction products, equation of state (EOS) for ideal-gas or real-matter option, laser light absorption and electron-ion relaxation. This code version (gotten ready to easily append the already prepared non-local alpha-particle deposition theoretical "diffusive" model), included a rough model for finite-range radiative transport description [14].

The basic physical models included in the above described 1-D code version, implemented with nonlocal alpha-particle deposition [15] and with cohesion effects in the real matter EOS treatment [16], have been adapted to a 2-D version [17] based on the numerical outline reported by Schulz [18].

The current versions CoMo3 and CoBi3, improved in the Von Neumann artificial viscosity [19] and in the real matter EOS numerical treatments, include a mesh correction based on a collisional method [20] and the option to choose as energy source a laser, heavy ions [21, 22], external thermal radiation [23, 24, 25], or macroparticle impact [1, 26]. A radiation transport model [27, 28] implemented with semi-empirical Planck and Rosseland opacities, taking into account, to some degree, the nonlocal thermal transport description, was also included.

CoMo3 and Cobi3 deal with a fluid formed of three different, coupled, atomic species:

- ions (average charge and atomic weight, locally thermalized to a single temperature);
- electrons (population determined by ionization equilibrium to their own local temperature);
- photons, obeying a Planck spectrum with a defined local temperature ("gray approximation").

These codes are the so-called "three-temperature" codes (ions, electrons and photons), but they can run also as 1T (neutral atoms), 2T (ions and electrons).

The alpha-particles may be treated when fusion reactions appear.

The system of the fluid dynamics equations, written (for plane, cylindrical or spherical symmetries) in a Lagrangian framework, is basically formed of the conservation-law equations of mass, momentum and energy.

The conservation equations are settled in a first-order "finite-difference" scheme, both for temporal and spatial description. The zoning (spatial discretization or mesh) is done by dividing the matter in large regions (macrozones) and then in layers (CoMo) or cells (CoBi). The macrozones can be used to divide different materials as well as different resolution zones.

The density is fully determined from the fluid particle volume, since the mass is conserved (losses due to the mass transferred alpha-particle, neutrons, etc. are neglected).

Since the inertia is neglected for all species but ions, the momentum conservation equation is reduced to an equation determining the fluid (ions) macroscopic velocity (one component for

CoMo, two for CoBi). In this equation, the terms describing the momentum transport due to electron flux or alpha-particle flux are also neglected.

The energy conservation is represented by a coupled set of equations, one for each species considered. Thermal fluxes are described by using the classical Fourier diffusion approximation with flux-limited effective conducibilities. For ions and electrons, the conducibilities are given by the standard theoretical plasma expressions [29, 30]. For electrons, a "free-streaming" flux-limiting correction is harmonically added to the classical conducibility. The flux limit is controlled by a parameter *fl,* relevant in this presentation, because of the experimental normalization discussed elsewhere.

The radiation conducibility is approximated by a semi-empirical expression that matches quite well, for the published cases, the opacity coefficients reported in the SESAME tables [31]. To a certain extent, the effects of a nonlocal thermal equilibrium with the electrons, as well as the "black-body" flux limit, are taken into account.

Ion-electron and photon-electron relaxation processes are also considered.

The EOS are needed to close the fluid model. For these codes, they are written so as to give the pressure, energy, specific heat and the density derivative of the energy, for each main species, once the respective temperature and mass density are known.

The codes can simulate the interaction between the matter and a laser, a heavy-ion beam, an external radiation field or an external pressure. A temporal evolution can be assigned to the chosen driver, by different predetermined analytic functions or by data arrays. For CoBi, the spatial distribution of the energy density can also be assigned among different analytic profiles and, in the case of laser-matter interaction, the effect of the localization system may be included. Energy absorption is computed along trajectories prescribed by a ray-tracing algorithm [32], with assigned focus position and convergence.

As a by-product of the experiments previously described (see sec. 1.1), some hints on the normalization of our Lagrangian 1-D and 2-D codes (CoMo3 and CoBi3) were searched for, especially with reference to the electronic heat transport description.

Since in codes such as CoBi3 the electronic thermal conductivity is described in terms of a flux-limited model, the experiments allow the determination of the flux limiter from the value of the maximum foil displacement and from its shape.

The dense phase displacement, as predicted by CoBi3 for three different values of the flux limiter, was performed for a thin SiO_2 square foil (4 μm thick) irradiated by a laser pulse, as described in figure 1a and 2a. Comparison with the experimental dense phase displacement profile allows selection of the proper value of the flux limiter. Only for a value *fl* does the shape agree with the profiles experimentally observed.

Figures 15a and 15b report as an example, the sensitivity of the theoretical dense phase profile to the value of the flux limiter.

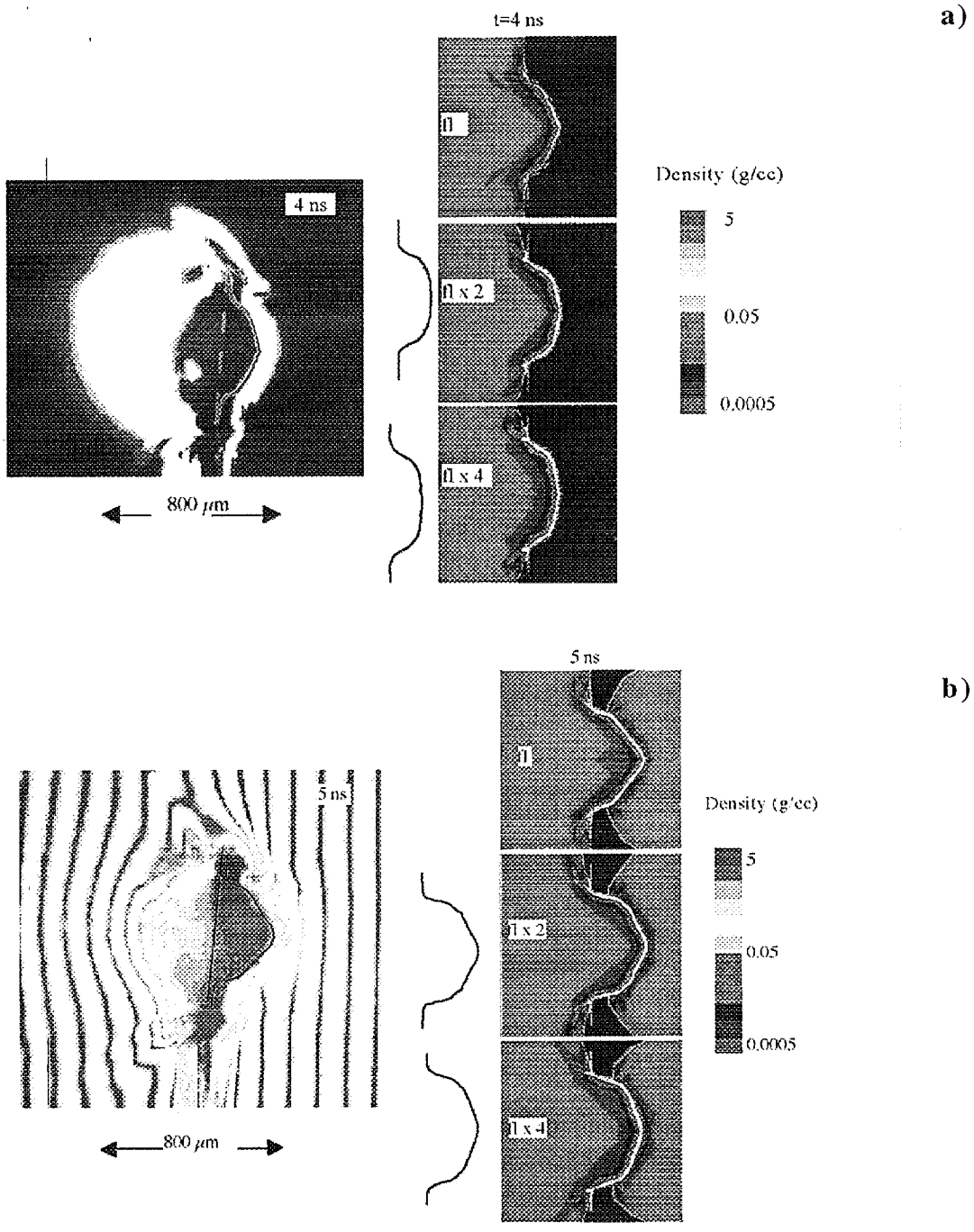

*Fig. 15 - Dense phase displacement as predicted by code **CoBi3** for three different values of the flux limiter. These simulations were performed for the laser pulse and the focusing conditions described in fig. 1a and fig. 2a. Only for a value* **f**l *does the shape agree with the profiles experimentally observed at 4 ns (a) and 5 ns (b). The straight line represents the initial target position*

2. THEORETICAL AND NUMERICAL ACTIVITY

2.1. Theoretical studies on gain of laser-compressed DT fuel ignited by external injected triggers (A. Caruso)

Theoretical studies have been made [1] to estimate gain and trigger conditions for a scheme in which heavy ions, x rays, or macroparticle impact are used to ignite a laser compressed cold fuel. The value of this scheme, in the framework of energy production, was compared with the conventional scheme, where ignition is provided by a central hot spot formed by the implosion process itself.

The trigger-energy values used in the gain evaluations were deduced by extensive theoretical investigations. As an example, to ignite a 200 g/cm^3 DT fuel the burst of a 40-kJ ion beam (15 GeV Bi) or a 12-kJ gold macroparticle (0.97 μg, velocity=5×10^8 cm/s) seems to be sufficient. From these studies are deduced the characteristics of the new trigger drivers required for these applications. As the laser energy used for compression is much larger than the trigger energy, it is possible to adopt triggering drivers much less efficient than the laser used for fuel compression, and yet satisfy reactor loop conditions.

In the following, some conclusions of the studies extensively discussed in [1] are reported.

The spark-injection scheme seems promising for gains adequate for energy production. The gain can be so high as to make the existing laser efficiency almost sufficient for compressing DT fuel in reactor conditions (not repetition rate).

This approach however requires the development of entirely new drivers specialized to ignition at energy levels of 10÷50 kJ.

One possibility is to develop extremely low-emittance, ultra-short heavy-ions generators.

The use of an x-rays burst for ignition is another possibility. The photon energy should be about $114\sqrt{\rho}$ eV, where ρ is the fuel density (in g/cm^3).

The development of macroparticle accelerators should be revisited in view of this new analysis of the ICF scheme. Actually, it is now clear that the required particle energies are around 10 kJ for particle masses of less than 1 μg. Revisiting is also suggested by the continuous advances in many technologies.

Another important point to be noted is the possibility of making the trigger energy E_{tr}<<*laser energy* used to compress the fuel (E_{las}). For relevant examples, an energy ratio as small as $E_{tr}/E_{las} \approx 0.012$ has been found. This feature makes the trigger driver efficiency not relevant in reactor considerations, until the laser and the triggering driver efficiencies satisfy the condition

$$\eta_{tr} > (E_{tr} / E_{las})\eta_{las}$$

2.2 Numerical studies on the ignition of dense DT fuel by external injected triggers (A. Caruso, V. A. Pais)

One- and two-dimensional numerical simulations have been performed [26] by using the CoMo3 and CoBi3 Lagrangian hydrodynamic codes (see sec. 1.3).

The cold fuel assembly was assumed as formed and the relevant ignition criteria were searched for.

The cases considered are those in which the ignition spark has been formed by a short pulse of 15-GeV Bi ions or by a gold-macroparticle impact. Targets of different shapes and densities were studied.

The heavy-ion energy beam necessary for ignition scales with the fuel density in the conventional way ($\propto 1/\rho^2$). This follows from the assumption of total beam energy transfer to the fuel and from the requirement of having a spark sized on the alpha-particle range at a temperature of about 5-7 keV.

Numerical simulations with the CoMo3 and CoBi3 codes were performed to normalize the $1/\rho^2$ dependence and to produce an ignition energy estimate.

The ignition energy per unit surface was first evaluated by 1-D studies for the ignition of DT half-spaces at 200 g/cm^3. The energy density values leading to ignition were then used as input for the 2-D calculations where a finite irradiation spot was introduced. In this case, cylinders of fuel with dimensions much greater than the heavy-ion spot were used as targets. The heavy-ion beam also had a cylindrical geometry, coaxially impinging onto the target. Again modified Gaussian profiles were adopted for power time dependence, whereas truncated Gaussian profiles were used for the ion beam space distribution (maximum beam radius=2xbeam radius at 1/e of maximum power density).

The ignition energy per unit surface over the whole spot in the 2-D calculations turned out to be about a factor 3 greater than that in the 1-D simulations for the corresponding case.

Figures 16 and 17 show the temperature maps at three different instants for a case in which ignition fails and for one in which ignition occurs. The results of these studies are summarized by the formula

$$E_{tr} = 40\left(\frac{200}{\rho}\right)^2 \text{ kJ},$$

where ρ in g/cm^3.

In addition to these studies, ignition was produced in a fuel in which the physical conditions (field of density, velocity etc.), at the beginning of the interaction with a parallel, cylindrically

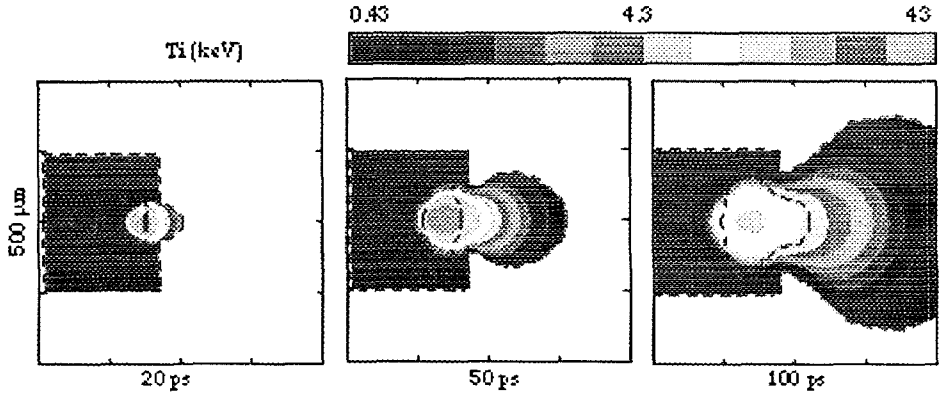

Fig. 16 - 2-D ion beam irradiation without ignition. Three instants of the evolution of a DT cylinder (240 μm diameter x200 μm length) at 200 g/cm^3, triggered by a 15GeV Bi ion beam impinging coaxially onto it. The cylindrical beam (maximum radius of 30 μm) is unfocused and the associated total energy is 30 kJ. The FWHM duration is 10 ps and the power time dependence again follows a modified Gaussian profile. The colors in the figures indicate ionic temperatures as by the included scale. Note the formation of the hot-spot and the subsequent cooling.

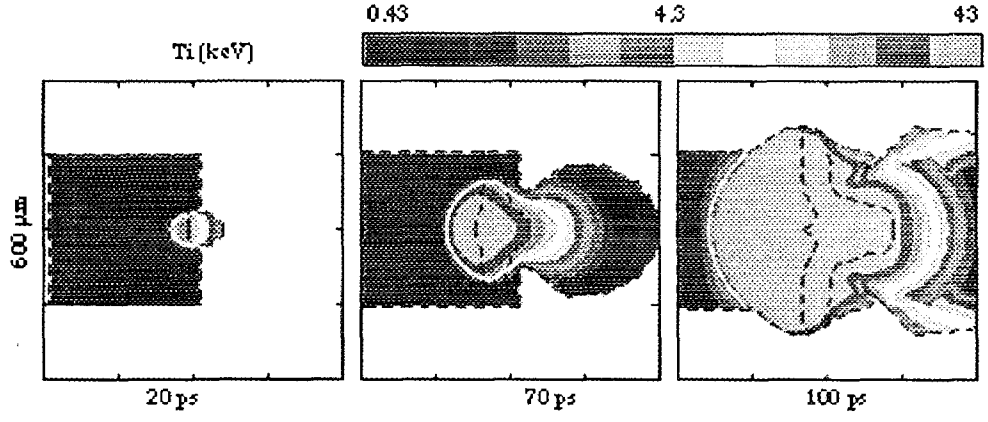

Fig. 17 - 2-D ion beam irradiation with ignition. Three instants of the evolution of a DT cylinder (300 μm diameter x 300 μm length) at 200 g/cm^3, triggered by a 15 GeV Bi ion beam impinging coaxially onto it. The beam having cylindrical geometry (maximum radius of 30 μm) is unfocused and the associated total energy is 40 kJ. The FWHM duration is 10 ps and the power time dependence again follows a modified Gaussian profile. The colors in the figures indicate ionic temperatures as by the included scale. Note the propagation of the self-sustained burn wave with the consequent growth of the heated volume.

symmetric heavy-ion beam, were those computed, near stagnation, for the 1-D laser implosion of a single empty spherical DT shell.

The main parameters were the following: laser energy=1 MJ, shell aspect ratio 10, final average fuel density≈100 g/cm^3, heavy-ion pulse energy=100 kJ, heavy-ion pulse duration (FWHM)= 100 ps, maximun beam radius=30 μm. The overall energy gain was greater than 300.

Figures 18a, 18b, 19a and 19b show temperature and density maps during the ignition and burn processes.

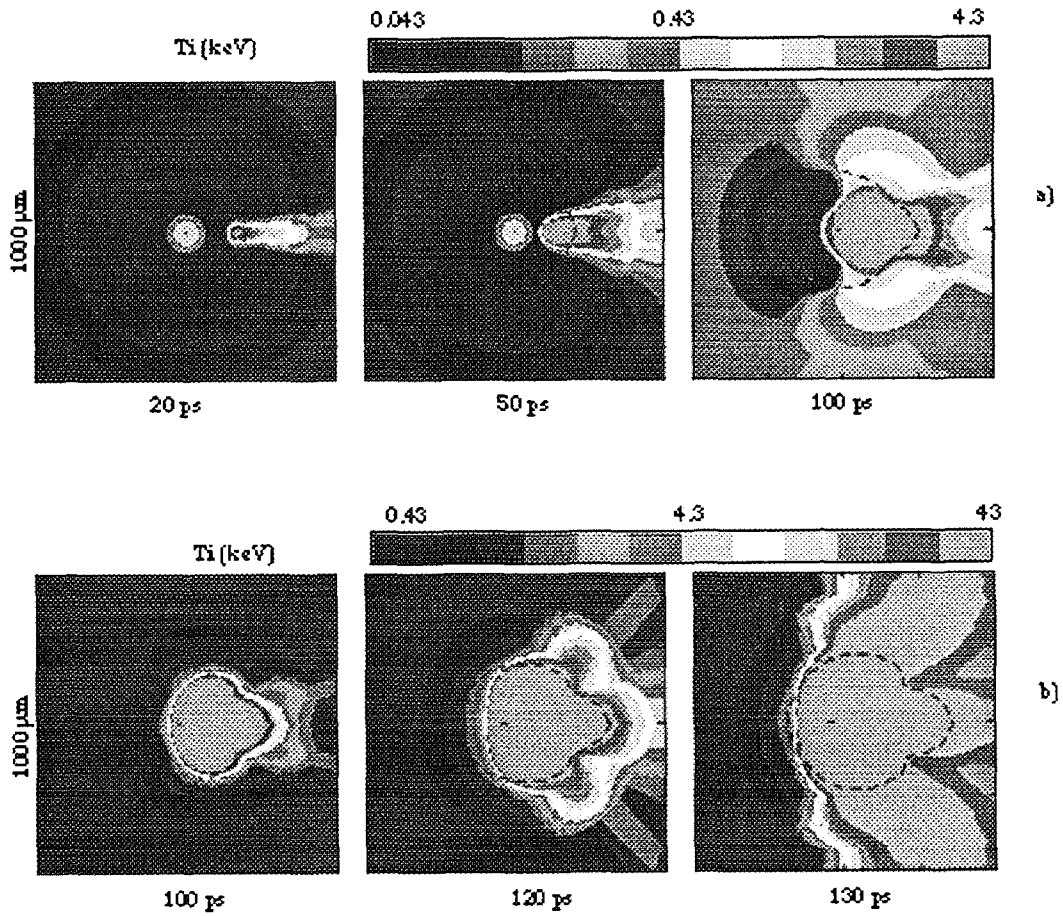

Fig. 18 Ignition of a laser spherically compressed fuel triggered by a 15-GeV Bi ion beam pulse: ion temperature maps. The initial conditions are those computed with the 1-D code near stagnation. This implosion is produced with a 0.353-μm wavelength, properly shaped laser pulse of 1 MJ total energy and 100 ns total duration. The target is a spherical solid DT shell of 2600 μm average radius and 280 μm thickness. The trigger beam energy is 100 kJ, released in 100 ps (FWHM), cylindrical (maximum beam radius 30 μm), unfocused, and coaxial with a target diameter. At stagnation, the high-density fuel is located within the dashed circle with the corona remnant distributed outside. The colors in the figures indicate ionic temperatures as by the included scale. The (a) sequence illustrates the ignition evolution while the (b) sequence shows the subsequent burn evolution. The overall energy gain exceeds 300.

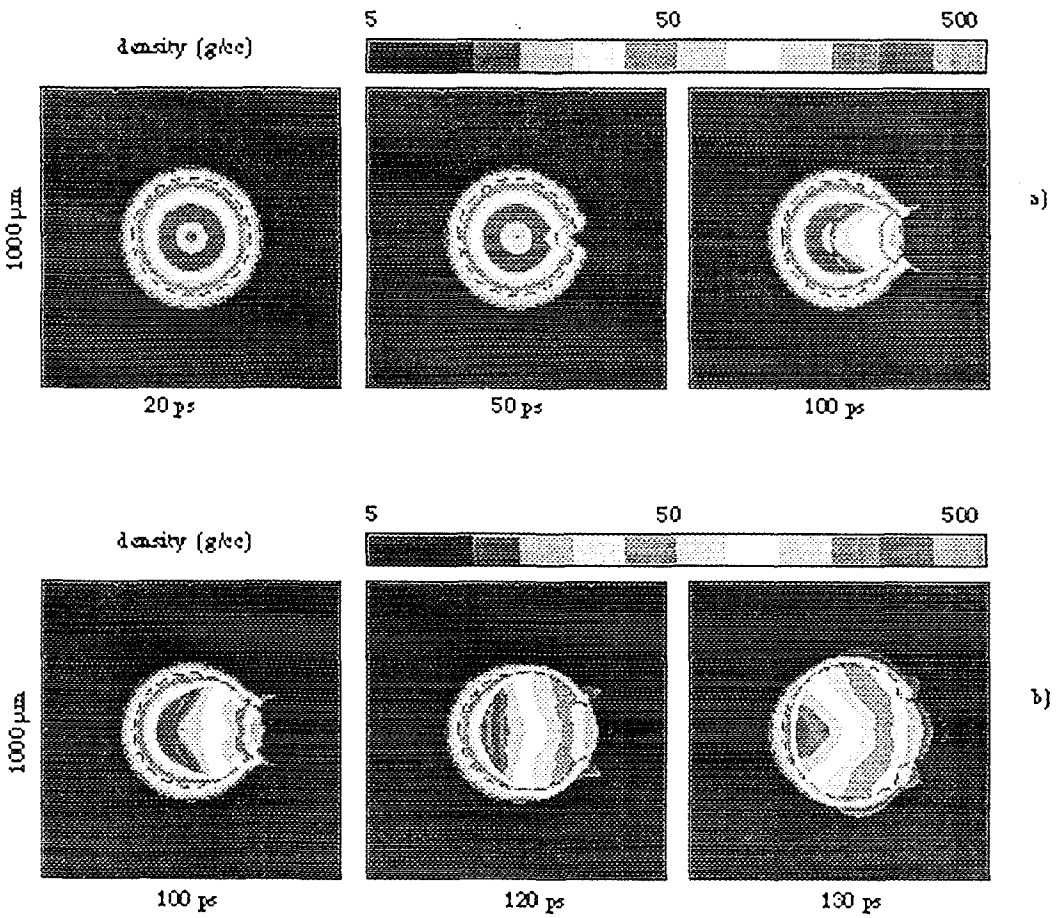

Fig. 19 Ignition of a laser spherically compressed fuel triggered by a 15-GeV Bi ion beam pulse (the same case as figure 18): density maps.

A study was also performed to normalize a theoretical formula [1] for the ignition energy in the case of macroparticle impact. The strategy adopted was similar to that used for heavy ions.

Exploratory 1-D simulations were first performed to determine the main parameters (i.e. macroparticle velocity and thickness) to be used for the final 2-D simulations.

The impact of a 40-µm-long, 40-µm-diam gold cylinder on a DT half-space at density 200 g/cm^3 was then studied by 2-D simulations. No ignition occurs at a velocity of 4×10^8 cm/s. Ignition is obtained by raising the velocity to 5×10^8 cm/s. The threshold energy is about 12 kJ, corresponding to a macroparticle mass of 0.97 µg. An example of ignition by macroparticle impact is shown in figures 20a,b and 21a,b.

This case was used for normalizations in order to produce the final estimate for trigger energy [1] given by

$$E_{tr} = 3.5 \times 10^3 \, a(1+a)^2 \, \frac{1}{\rho^2} \quad \text{kJ}$$

In this formula $a = \sqrt{4\rho / 3\rho_{MP}}$ where ρ_{MP} is the impinging macroparticle density and densities are in g/cm^3.

For macroparticle impact, the ignition energy per unit surface in 2-D calculations is about a factor 1.6 higher than that required in the corresponding 1-D calculations.

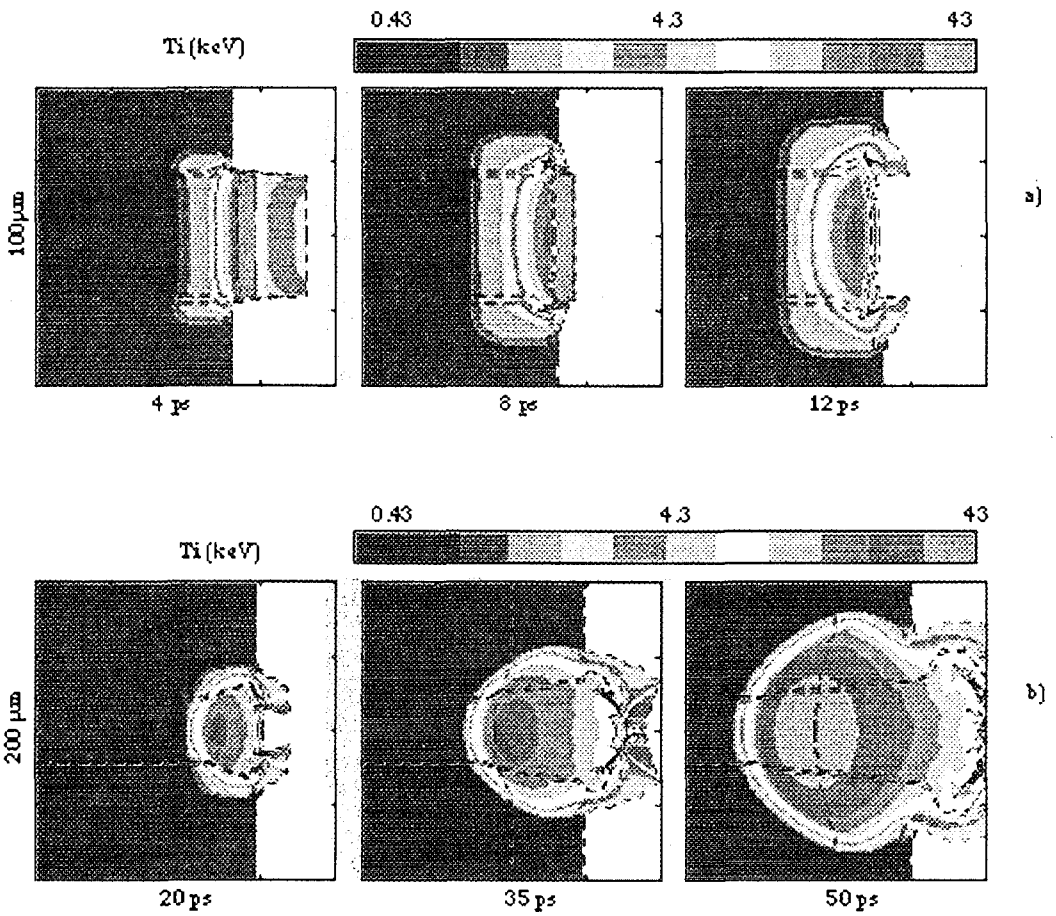

Fig. 20 - Ignition by macroparticle impact. A gold cylinder (diameter=length=40 µm, velocity=5.x10^8 cm/s) collides coaxially with a 200 g/cm^3 DT cylinder (diameter=length=300 µm). (a) three instants of the evolution around the initial interaction stages (100 µm x 100 µm field); (b) three instants of the evolution of the ignition process (200 µm x 200 µm field). The colors in the figures indicate ionic temperatures as by the included scale. Note the evolution of the collision, the collapse of the macroparticle and the propagation of the self-sustained burn wave.

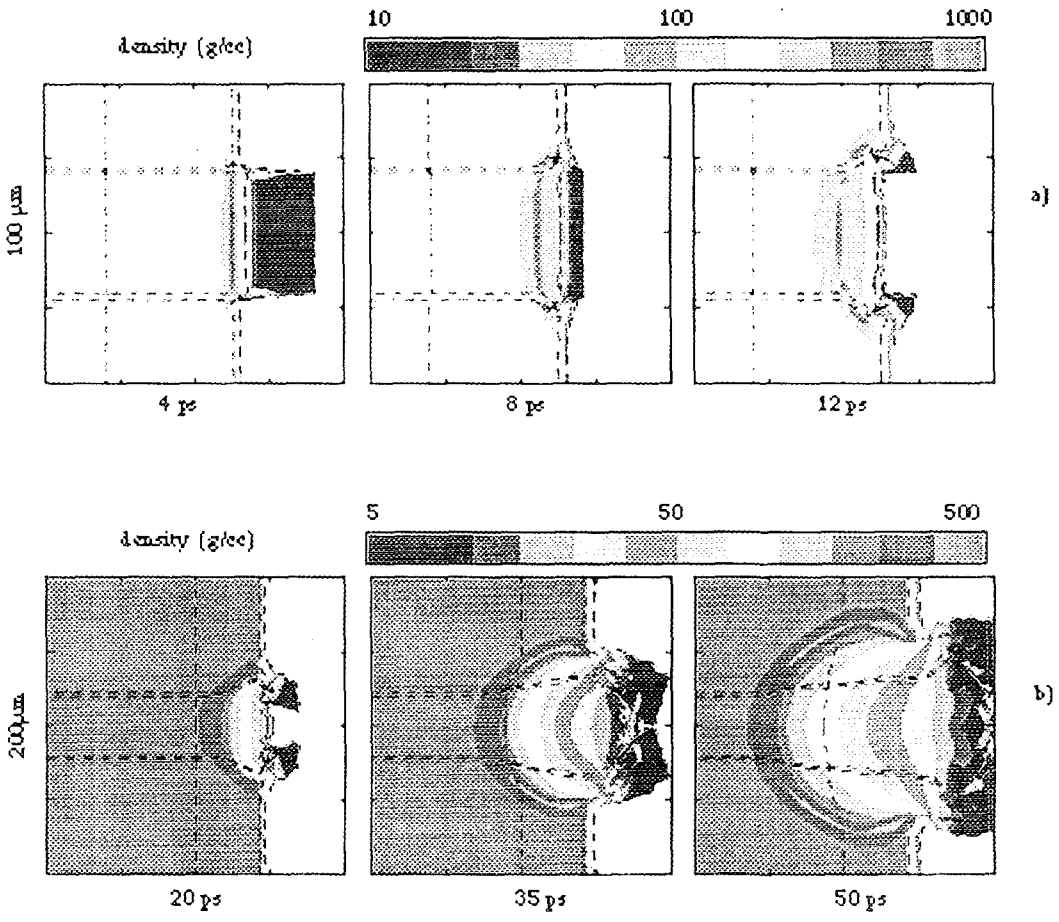

Fig. 21 - Ignition by macroparticle impact (same case as fig. 20). The colors in the figures indicate ionic temperatures as by the included scale. Comparison with fig. 20 completes the physical insight of the evolution. The crater formed by the ignition is also to be appreciated.

REFERENCES

[1] A. Caruso: Proc. of the IAEA Technical Committee Meeting on Drivers for Inertial Confinement Fusion, Paris, 14-18 /11/1994.

[2] M. Tabak et al.: LLNL ICF Quarterly Report Vol. 4, N. 3 (1994).

[3] Ch. Maisonnier: Il Nuovo Cimento **42B**, 2, 332 (1966).

[4] A. Caruso: R. Gratton: Plasma Phys. **10**, 867 (1968).

[5] A. Caruso, R. Gratton: Plasma Phys. **11**, 839 (1969).

[6] A. Caruso et al.: Phys. Lett. **29A** 6, 316 (1969).

[7] P.L. Andreoli, A. Caruso, G. Cristofari, A. Di Paolo, P. Maci, C. Strangio: Inertial Fusion Progress Report (1992-1993), ENEA Report RT/ERG/FUS/93/67, Centro Ricerche di Frascati, 34, (1993).

[8] P.L. Andreoli, A. Caruso, G. Cristofari, D. Iavarone, P. Maci, C. Strangio: Inertial Fusion Progress Report (1992-1993), 46.

[9] C. Strangio, A. Caruso: Laser and Particle Beams **8**, 1-2, 135 (1990) and ENEA Report RT/FUS/88/18 (1988).

[10] P. L. Andreoli, A. Caruso, G. Di Giorgio, M. Falzano, C. Strangio, M. Torbidoni, Inertial Fusion Progress Report (1992-1993), 49.

[11] C. Strangio, A. Caruso: "Study on the hydrodynamical behaviour of thin foils irradiated by near field ISI smoothed beams", to be published in Laser and Particle Beams.

[12] A. Caruso et al: "Interaction experiment with ISI smoothed beams on the ABC facility", to be pubblished in Proc. XXIV ECLIM, Madrid (1996).

[13] A. Caruso, P. Giupponi: unpublished (1977).

[14] A. Caruso: Plasma Phys. **16**, 683 (1974).

[15] S. Atzeni, Thesis: "Sull'ignizione termonucleare controllata di combustibile solido irraggiato con fascio laser", University of Rome unpublished (1979).

[16] S. Atzeni, A. Caruso, V. A. Pais: Laser and Particle Beams, **4**, 393 (1986).

[17] S. Atzeni, P. Giupponi: ENEA Report RT/FUS/84/9, Centro Ricerche di Frascati (1984).

[18] W. D. Schulz: Methods in Computational Physics, Vol. 3, eds. B. Alder, S. Ferubach and M. Rotenberg (Academic Press, New York, London) (1964).

[19] V. A. Pais, D. Pacella: Il Nuovo Cimento, **100B** 6, 781 (1987)

[20] V. A. Pais, A. Caruso: Comp. Phys. Commun. **58**, 55 (1990).

[21] A. Caruso, V. A. Pais: Il Nuovo Cimento, **13D**, 969 (1991).

[22] A. Caruso, V. A. Pais, A. Parodi: Laser and Particle Beams **10**, 447 (1992).

[23] A. Caruso and V. A. Pais: Int. School of Plasma Phys. "Piero Caldirola", Varenna, Italia, 6-16/9/1988, Commission of the European Communities, EUR 11930 EN.

[24] A. Caruso, V. A. Pais: Laser and Particle Beams, **11,** 157 (1993).

[25] A. Caruso, V. A. Pais: Laser and Particle Beams, **12,** 343 (1994).

[26] A. Caruso, V. A. Pais: Nuclear Fusion, **36**, 6, (1996)

[27] A. Caruso, A. Dattola: unpublished (1981).

[28] A. Dattola: Thesis "Ignizione di combustibili avanzati e trasporto della radiazione nella Fusione a Confinamento Inerziale", University of Rome, unpublished (1982).

[29] L. Spitzer jr.: Physics of Fully Ionized Gases, Wiley & Sons, 2nd ed., New York, (1967).

[30] D. L. Book: NRL Plasma Formulary, NRL Memorandum Report 3322.

[31] Los Alamos Equation of State And Opacity Group, Theoretical Division 1983, Los Alamos National Laboratory, Report LALP-83-4.

[32] A.Friedman: LLNL Annual Report, p.3, (1983).

Edito dall' ENEA
Unità Comunicazione e Informazione
Lungotevere Grande Ammiraglio Thaon di Revel, 76 - 00196 Roma
Stampa: Centro Stampa Tecnografico - C. R. Frascati

Finito di stampare nel mese di dicembre 1997